



Enhanced Removal of Eriochrome Black T Using Graphene/NiMgAl-Layered Hydroxides: Isotherm, Kinetic, and Thermodynamic Studies

Taye Saheed Kazeem¹ · Mukarram Zubair² · Muhammad Daud³ · Mamdouh A. Al-Harthy^{1,4}

Received: 31 March 2019 / Accepted: 30 December 2019 / Published online: 16 January 2020
© King Fahd University of Petroleum & Minerals 2020

Abstract

In this study, graphene (G) was used as a substrate for NiMgAl ternary-layered hydroxide using coprecipitation technique. The pristine NiMgAl (NMA), graphene-NiMgAl (G/NMA) and their respective calcined products NMA-C and G/NMA-C were investigated as adsorbents for the removal of hazardous eriochrome black T (EBT) dye from an aqueous phase. Characterization results revealed that the incorporation of graphene nanoparticles with NMA with subsequent calcination leads to a significant improvement in surface functionalities, thermal stability, and specific surface area. This resulted in high and fast uptake of EBT molecules from the water phase. The equilibrium time for NMA, NMA-C, G/NMA, and G/NMA-C was achieved at 240 min, 180 min, 90 min, and 60 min, respectively, with optimum pH 4 and dosage of 10 mg. The Langmuir isotherm model describes the adsorption process more appropriately with maximum achievable adsorption capacities of 156.25, 263.16, 238.14, and 384.62 mg/g for NMA, G/NMA, NMA-C, and G/NMA-C, respectively. The kinetic study indicates the adequacy and fitness of the pseudo-second-order model to the experimental data for all four adsorbents. The thermodynamic evaluation substantiates the exothermic nature of the adsorption processes. The mechanism of EBT-G/NMA-C adsorption system involved surface adsorption, electrostatic, strong chemical, and ion exchange interactions along with surface reconstruction. Integration of graphene with subsequent calcination substantially improved the surface and structure characteristics of NMA which facilitated enhanced adsorption performance with sorption rate and excellent reusability performance, confirming it as a highly promising adsorbent for the efficient remediation of dye-contaminated wastewater.

Keywords Graphene · Ternary-layered double hydroxide · Dye removal · Isotherm and kinetic studies

Electronic supplementary material The online version of this article (<https://doi.org/10.1007/s13369-019-04327-2>) contains supplementary material, which is available to authorized users.

✉ Mamdouh A. Al-Harthy
mamdouh@kfupm.edu.sa

¹ Department of Chemical Engineering, King Fahd University of Petroleum & Minerals, Dhahran 31261, Saudi Arabia

² Department of Environmental Engineering, Imam Abdulrahman Bin Faisal University, Dammam 31982, Saudi Arabia

³ Department of Chemical Engineering, University of Engineering and Technology, Peshawar 25120, Pakistan

⁴ Center of Research Excellence in Nanotechnology, King Fahd University of Petroleum and Minerals, Dhahran 31261, Saudi Arabia

1 Introduction

Azo dyes are some of the world most demanded products due to their extensive use in textiles, printing, paints, plastic industries and account for more than 60% of total world dye usage [1]. More than 700,000 tonnes of these dyes is produced worldwide, and about 15% of them find a way into water bodies as effluents [2]. Their disposal in the environment has generated a lot of health, socio-economic, and environmental concerns due to their potential antiaesthetic, carcinogenic, and biotoxic effects [3]. The recalcitrance of azo dyes to biodegradation has motivated research into physicochemical techniques such as solvent extraction, ion exchange, membrane filtration, evaporation [3] to comply with stringent regulation on the allowable limits of dye concentration in the discharged effluent. Adsorption technique is an affordable, easy, and efficient process for removing dyes from the aqueous phase [4, 5].



Utilization of proper adsorbent material is one of the crucial steps for effective decontamination process. A lot of adsorbents were previously utilized for dye-contaminated water remediation among which are activated carbon, bentonite, zeolite, etc. Due to high production cost and low sorption performance, researchers are expending extensive efforts to produce new eco-economic adsorbents, exhibiting high removal efficiencies.

Layered double hydroxides (LDHs), also termed as hydrotalcites, have huge applications in water remediation due to excellent properties of high specific surface area and ion exchange capacity [6]. LDHs derived from parent mineral $Mg_6Al_2(OH)_{16}CO_3 \cdot 4H_2O$ are a member of the family of 2D nanostructured anionic clays which possess hydrotalcite morphology and characterized by a positively charged host and charge-balanced by substitutable interlamellar anions. LDHs possess unique structural formula of $[M_{1-x}^{2+}M_x^{3+}(OH)_2]^{x+}(A^{n-})_{x/n} \cdot mH_2O$ [7, 8]. M^{3+} stands for trivalent cations, while the M^{2+} represents the divalent cations and A^{n-} is the interlayer anions and n has been reported to lie between 0.22 and 0.33 [8]. Intercalation of various materials (carbon nanomaterials, polymers, anions, etc.) into layered double hydroxides has been reported as a promising approach for a significant improvement in properties of LDHs.

For wastewater treatment, carbon nanostructures such as amorphous carbon [9], carbon nanotube [10], multi-walled carbon nanotubes [11], carbon dot [12], and graphene [13] were reported as a suitable support for LDHs for outstanding adsorption performance. Particularly, high specific surface area ($\sim 2700 \text{ m}^2/\text{g}$) has attracted graphene as a potential candidate for the treatment of toxic dyes in wastewater [8]. Previously, graphene/LDH composites have been investigated and exhibited superior physical properties when compared to either LDHs or graphene [14]. Graphene/LDH nanohybrids also revealed outstanding remediation of anionic and cationic dyes wastewater [8]. Ternary LDHs, comprising three metallic ions, have been recently exploited, and they revealed superb removal efficiency of dyes from the aqueous phase. For instance, Bharali and Deka demonstrated the high adsorptive property of CuMgAl LDH for the removal of both anionic and cationic dyes [15]. They reported an increase in removal efficiency of methyl orange (MO) dye with increased Cu^{2+} composition ratio despite the reduction in surface area. They proposed that Cu^{2+} ratio induces lower basicity which contributed to the attraction between the dye molecules and LDH surface. Likewise, Zaghouane et al. [16] removed methyl orange effectively from the aqueous phase using uncalcined and calcined MgNiAl LDHs. Other studies also reported ternary-layered double hydroxides as promising adsorbents for adsorption of dyes [17, 18]. Previous studies have revealed that coupling of LDHs with graphene as a substrate [19, 20] not only prevented aggregation of the LDHs but also leads to a significant enhancement in

surface area and formation of mixed metal oxides after subsequent calcination. Based on detailed literature, up to date, the coupling of ternary LDHs with carbon nanostructures such as graphene has for wastewater treatment limited studies. Therefore, it is expected that intercalation of graphene with ternary LDHs may result in improved surface characteristics, stability and facilitate the adsorption of dyes from the water phase.

The focus of this study was to assess the removal potential of azo dyes from aqueous solution by facilely synthesized ternary LDH and graphene/ternary LDH composite. Eriochrome black T (EBT) was chosen as a model dye due to its recalcitrance to chemical and biological degradation. FTIR, XRD, BET SEM, TEM, and TGA analyses were used to characterize the composites to reveal their physico-chemical properties. Effects of various influential parameters such as pH, contact time, dosage, and temperature on EBT removal were performed in batch experiments. The adsorption equilibrium data were analyzed using isotherm models, while time dependence was fitted to kinetic models. In addition, the mechanism behind the adsorption was proposed. Furthermore, regeneration of the spent adsorbent was investigated to evaluate its potential for industrial application. The uncalcined NiMgAl, calcined NiMgAl, uncalcined graphene-NiMgAl, and calcined graphene-NiMgAl are referred to as NMA, NMA-C, G/NMA, and G/NMA-C, respectively.

2 Materials and Methods

2.1 Materials

Aluminum nitrate nonahydrate ($Al(NO_3)_3 \cdot 9H_2O$), magnesium nitrate hexahydrate ($Mg(NO_3)_2 \cdot 6H_2O$), and nickel nitrate hexahydrate ($Ni(NO_3)_2 \cdot 6H_2O$) were purchased from Sigma-Aldrich Co. (Germany). Graphene (GRAFEN[®]-SEG/Semi-exfoliated Graphene Sheets) was procured from GRAFEN future engineering (Ankara, Turkey). NaOH and HCl were purchased from PanReac AppliChem (Darmstadt, Germany) and EUROSTAR (Liverpool, UK), respectively. All the solutions were prepared using deionized water.

2.2 Synthesis of Ternary LDH and Graphene/Ternary LDH Composite

The ternary LDH (NMA) was synthesized via coprecipitation technique as described by other authors with a slight adjustment [21]. About, 0.02 mol of $Al(NO_3)_3 \cdot 9H_2O$, 0.02 mol of $Ni(NO_3)_2 \cdot 6H_2O$, and 0.04 mol of $Mg(NO_3)_2 \cdot 6H_2O$ (total ratio of M^{2+} to M^{3+} is 3) were dissolved in 60 mL of deionized water in a 500-mL round-bottom flask. The mixture was stirred vigorously at 600 rpm in an oil bath at 60 °C for



15 min. Subsequently, 1 M NaOH was added dropwisely to stabilize the pH at 10 ± 0.5 while maintaining the stirrer speed and temperature of 60 °C. Thereafter, the temperature was raised to 90 °C and stirring increased to 900 rpm, while the reaction was refluxed for 24 h. The suspension obtained was subjected to centrifugation and washed twice with deionized water and then followed by twice washing using ethanol to remove impurities. The densely obtained slurry was dried in a vacuum oven at 90 °C for 24–48 h.

For the preparation of graphene/ternary LDH composite, 300 mg of graphene was added to 60 mL NaOH (0.2 M) and the mixture was ultrasonicated at 60 rpm for 90 min. The obtained mixture was then added to a prepared mixture of the ternary LDH precursor, and two to three drops of hydrazine were added as a complexing agent. Other procedures were followed as outlined in the synthesis of NMA. Both ternary NMA and G/NMA were calcined at 400 °C for 3 h under 120 mL/min N_2 environment to produce NMA-C and G/NMA-C, respectively, and stored for use in adsorption experiment.

2.3 Characterization

XRD reflection patterns of the NMA, G/NMA, NMA-C, and G/NMA-C were obtained by utilizing Rigaku Miniflex II utilizing Cu K α monochromatic radiation ($\lambda = 0.15406$ nm, 40 mA, 30 kV) with a step size of 0.03 and scan rate of 3 scans/min with a range of 5–70° 2θ . The morphologies of the LDHs were obtained by scanning electron microscopy using TIMA TESCAN SEM Integrated system. The FTIR spectra were recorded by Nicolet 6700 spectrometer. BET analyzer (Micrometrics, Tristar II series) was used to determine the specific surface area, pore volume, and pore radius. Thermogravimetry analysis (TGA) was carried out using SDT-Q600 instrument by heating dry powder at 10 °C/min.

2.4 Preparation of EBT Solution

In total, 1000 mg/L stock solution of EBT dye was obtained by dissolving 1 g of EBT dye into 1 L of deionized water. Other concentrations were obtained by diluting to a required concentration of 40 to 200 mg/L.

2.5 EBT Adsorption Studies

Batch adsorption studies of EBT onto the composites were carried out to investigate the effects of important parameters such as pH, contact time, adsorbent dosage, initial dye concentration, and temperature. Nearly, 10 mg of each adsorbent in 30 mL of 40 mg/L EBT solution was agitated for 15–300 min on a shaker (Lab Companion SK-600 Benchtop, 120 VAC, 60 Hz, 0.4 A) set at 180 rpm. The shaker which has a coupling of water bath and thermostat allows

temperature control (25, 35, and 50 °C for this study) of the adsorption process. The required pH (2–9) of the mixture was obtained using 0.1 M NaOH or 0.1 M HCl solution with a HANNA (HI 2211) pH/ORP meter. After agitation, the adsorbent and adsorbate were separated by centrifugation set at 3500 rpm for 5 min. The final concentration of EBT was calculated from the area under the curve of maximum absorbance (425–707 nm) by JASCO V-670 UV–visible spectrometer. The percentage dye removal (%), time-dependent adsorption capacity (q_t), and equilibrium adsorption capacity (q_e) were computed from the following equations [22]

$$\% \text{Dye removal} = \frac{C_o - C_e}{C_o} * 100 \quad (1)$$

$$q_t = \frac{C_o - C_t}{M} * V_s \quad (2)$$

$$q_e = \frac{C_o - C_e}{M} * V_s \quad (3)$$

where C_o , C_e , and C_t , respectively, represent initial, equilibrium, and time-dependent dye concentrations (mg/L). M and V_s are the mass of adsorbents (g) and the volume of dye solution used (L), respectively.

2.6 Adsorption Isotherms

The adsorption isotherm is an indication of the extent of distribution of adsorbate between the liquid phase and solid phases upon reaching equilibrium in the adsorption process [23]. In this study, three well-established isotherm models, Langmuir isotherm, Freundlich isotherm, and Temkin isotherm, are considered at three different temperatures. Langmuir isotherm which is based on monolayer adsorption assumes homogeneous adsorption sites with equal energy [24], and nonlinear form is given by

$$q_e = \frac{q_m K_L C_e}{1 + K_L C_e} \quad (4)$$

In linear form, Eq. 4 is expressed as

$$\frac{C_e}{q_e} = \frac{1}{K_L q_m} + \frac{C_e}{q_m} \quad (5)$$

where q_e is quantity of dye adsorbed (mg/g), C_e is the amount of dye adsorbed at equilibrium (mg/L), and the Langmuir constants q_m (mg/g) and K_L (L/mg) are the maximum monolayer adsorption of the adsorbent and relation to free energy of adsorption, respectively [25]. A consolidating parameter to determine the favorability or unfavorability of

the adsorption system is the essential factor (or separation factor), R_L , defined as

$$R_L = \frac{1}{1 + K_L C_0} \quad (6)$$

where $R_L > 1$ is unfavorable, $R_L = 1$ is linear, $0 < R_L < 1$ is favorable, and $R_L = 0$ indicate irreversible adsorption. C_0 is the highest initial dye concentration (mg/L).

Freundlich isotherm, which is appropriate for low concentration, assumes a heterogeneous surface with the heat of adsorption distribution [23] and mathematically represented as

$$q_e = K_F C_e^{1/n} \quad (7)$$

Linearization of Eq. 7 leads to

$$\log q_e = \log K_F + \frac{1}{n} \log C_e \quad (8)$$

K_F and n are Freundlich constants. n is an indication of adsorption intensity and extent of nonlinearity between adsorption and concentration of the solution and provides information on the favorability of adsorption, while K_F relates to the adsorption capacity [26].

Temkin isotherm [27] considers the adsorbate/adsorbent interaction where the heat adsorption reduces linearly with coverage for all molecules. In nonlinear and linear forms, it is represented, respectively, as

$$q_e = B \ln (A C_e) \quad (9)$$

$$q_e = B \ln A + Y \ln C_e \quad (10)$$

B is defined by

$$B = RT/b_T \quad (11)$$

$1/b_T$ defines the adsorbent/adsorption potential, T (K) is absolute temperature, and R is the gas constant.

2.7 Adsorption Kinetics

To predict feasible sorption process mechanism, adsorption rates were investigated using four kinetic models: pseudo-first-order (PFO), pseudo-second-order (PFO), intraparticle diffusion (IPD), and Elovich kinetic models shown in linearized forms Eqs. 12, 13, 14, and 15, respectively.

$$\log(q_e - q_t) = \log q_e - \frac{k_1 t}{2.303} \quad (12)$$

$$\frac{t}{q_t} = \frac{1}{k_2 q_e^2} + \frac{t}{q_e} \quad (13)$$

$$q_t = k_d t^{1/2} + C \quad (14)$$

$$q_t = \frac{1}{\beta} \ln(\alpha\beta) + \frac{1}{\beta} \ln(t) \quad (15)$$

where q_t and q_e are the time-dependent amount of dye adsorbed per unit of adsorbent (mg/g) during time contact time t (min) and at equilibrium, respectively, k_1 (1/min) is the pseudo-first-order rate constant, and k_2 (g/mg/min) is the pseudo-second-order rate constant. k_d (g/mg/min^{1/2}) represents the intraparticle diffusion rate constant. α (g/mg/min) and β (g/mg) denote initial adsorption and desorption coefficients, respectively. All parameters are obtained from the linear regression of their respective equations.

3 Results and Discussion

3.1 Characterization of NMA, G/NMA, NMA-C, and G/NMA-C

XRD patterns of the NMA, G/NMA, NMA-C, and G/NMA-C are displayed in Fig. 1a. Both the NMA and G/NMA exhibited high reflection peaks at 10.96°, 22.08°, and 34.77° with interplanar spacings of 8.06 Å, 4.02 Å, and 2.58 Å and corresponding to (003), (006), and (009) planes, respectively. The peaks at 38.75°, 45.7°, 60.89°, and 61.42° are assigned to (015), (018), (110), and (113) planes, respectively [16]. The result indicates the as-synthesized LDHs possess high crystallinity with well-layered structure. The additional peak observed in G/NMA at 26.46° corresponds to (002) plane associated with graphene crystallinity [28], indicating the presence of graphene in the LDH structure, and this may inherently improve its adsorption performance. It can be observed that the interlayer spacing did not increase in G/NMA; rather, graphene serves as a substrate for the LDH. Calcination led to the elimination of physisorbed and interlayer H₂O molecules as well as interlayer anions with a resultant collapse of the LDH lamellar structure. The result for the NMA-C and G/NMA-C shows the destruction of the LDHs structures after calcination with a resulting formation of mixed metal oxides MgO/NiO accompanied by the (200) and (220) planes [29]. Due to the relatively low temperature of calcination (below 600 °C), no peak was assigned to any aluminum oxide species such as spinel (MgAl₂O₄) which crystallizes at high temperature and it indicates dispersion of Al³⁺ into the solid matrix solution of MgO [30].

FTIR analysis contributes to understanding the functional groups on the active sites and the interactions among the groups influencing the adsorption. Figure 1b depicts the characteristic FTIR spectra of a typical LDH. The broad between 3300 and 3800 cm⁻¹ is associated with the

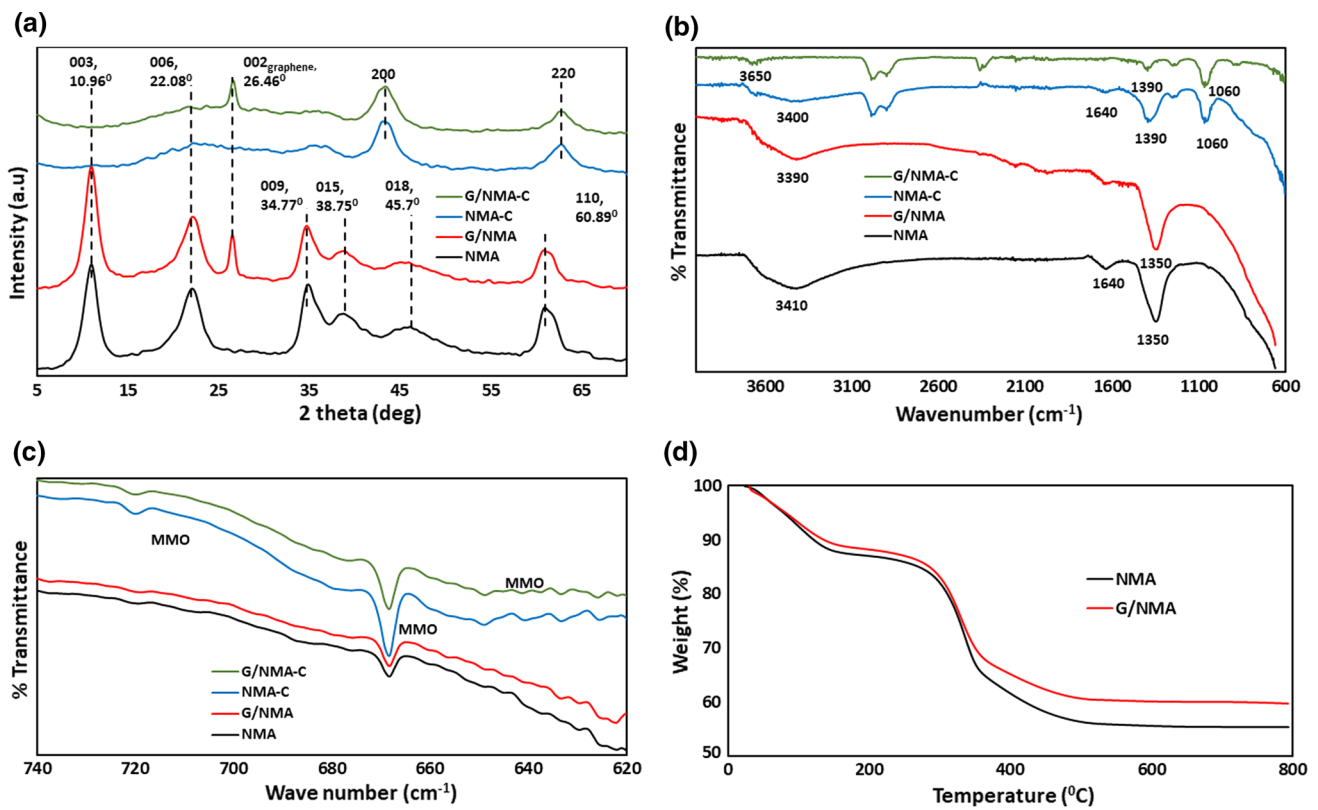


Fig. 1 X-ray diffractions (a), FTIR spectra for high range (b), FTIR spectra for low range (c), thermogravimetric analysis (d) of NMA, G/NMA, NMA-C, and G/NMA-C

stretching vibrations of OH group of interlayer H₂O in the brucite-like layers [31]. This band becomes [24] attenuated upon the calcination of the hydrotalcites as seen in the NMA-C and G/NMA-C. NMA and G/NMA have a weak band at 1640 cm⁻¹ corresponding to bending vibration of OH of water molecules and a strong band at 1350 cm⁻¹, indicating antisymmetric vibrations associated with nitrate ions. Though these bands become attenuated in NMA-C and G/NMA-C after calcination, they are not completely removed, indicating alteration of the structures of the LDHs (previously established from XRD). A new peak at 1060 cm⁻¹ corresponding to C–O–C bond appeared after calcination. In addition, the presence of stronger peaks at about 670 cm⁻¹ (Fig. 1c) in MCA-C and G/MCA-C indicates the abundant formation of mixed metal oxide (MMO) which has a profound impact on the adsorption performance.

Figure 1d depicts the thermogravimetric analysis (TGA) which shows the decomposition pattern and thermal stability of the LDH and its graphene hybrid. Three stages of weight loss occur under the thermal treatment up to a temperature of 800 °C. Physisorbed and intercalated water molecules are removed up to a temperature of 170 °C with a resultant weight loss of 11.5% and 10.5% for NMA and G/NMA, respectively. At the second stage, 23.5% for NMA

and 22% for G/NMA in weight loss occurred between 170 and 370 °C. This was due to decarbonation, dehydroxylation, and elimination of other interlayer anions [25]. The second weight loss resulted in the formation of mixed metal oxides (MMO). The thermal treatment above 370 °C with little weight loss led to continuous decarbonation and decarboxylation and more formation of MMO. The total weight loss upon thermal exposure suggests good thermal stability of the synthesized materials with G/NMA, possessing better and higher stability.

The BET surface area, pore volume, and average pore size of NMA, G/NMA, NMA-C, and G/NMA-C are listed in Table 1. The nitrogen adsorption–desorption isotherm plots

Table 1 Surface area, pore size, and pore volume of the NMA and G/NMA composites

	Surface area (m ² /g)	Pore size (Å)	Pore volume (cm ³ /g)
NMA	236.63	15.895	0.619
G/NMA	272.79	15.468	0.801
MCA-C	258.30	85.572	0.415
G/NMA-C	294.31	86.320	0.527

are displayed in Fig. S1 (supplementary data), and it represents type-IV isotherm (in accordance with IUPAC classification of adsorption isotherm) with hysteresis loop which is characteristic of mesoporous materials. This is evident in the pore size distributions of Fig. S2 (supplementary data) which show the materials contain predominantly mesopores. This is indicated in the average pore sizes which are 154.9 Å, 150.5 Å, 85.6 Å, and 86.320 Å for NMA, G/NMA, NMA-C, and G/NMA-C, respectively. The adsorbent materials are characterized by high surface areas which are significant for adsorption. Addition of graphene resulted in an increase in surface area from 236.63 to 272.79 m²/g depicting an increment of about 16%. In addition, the surface area of NMA and G/NMA upon calcination was increased to 258 m²/g and 294.31 m²/g, respectively. Due to the synergistic contribution of both calcination and graphene introduction, G/NMA-C possesses the highest surface area of 294.31 m²/g. Such synergistic contributions have been previously reported with respect to Cr(IV) sorption by calcined G-MgAl LDH [19]. Thus, G/NMA-C is expected to have profound uptake of EBT anions which can make it a potential superb sorbent material for the treatment of dye-contaminated wastewater.

Figure 2a–d shows the SEM microstructures of the as-synthesized NMA, G/NMA, NMA-C, and G/NMA, respectively. As shown in Fig. 2a, the surface of NMA comprises of tiny particles which aggregate to form a coarse platelet morphology. The SEM image of G/NMA showed that the

incorporation of graphene into the layers of NMA transformed the surface morphology of NMA into a highly porous and smooth surface. This is attributed to the overlapping and uniform dispersion of the graphene nanosheets within NMA layers. Similar behavior was also reported after the addition of graphene into MgCoAl LDH [32]. As expected, after calcination, the G/NMA-C morphology has completely changed to rough, compact, and homogeneous surface with nanoparticles. The compact nature is accompanied by a tighter pore (as previously established from average pore size values). The TEM images in Fig. 2e–f show the presence of nanosheet-like morphology of G/MCA with homogeneous dispersion of irregular plate-like LDH on the graphene. The homogenous dispersion contributed to the observed higher porous surface area of the composite material. Therefore, the presence of graphene nanoparticles with subsequent calcination provided a substantial improvement in the surface structure of ternary LDH which resulted in a significant enhancement in the removal performance of anionic dyes from the water phase.

3.2 Adsorption Parameters

3.2.1 Effect of Initial pH

The surface charge, as well as the degree of ionization of adsorbates and the adsorbent, is influenced by the solution

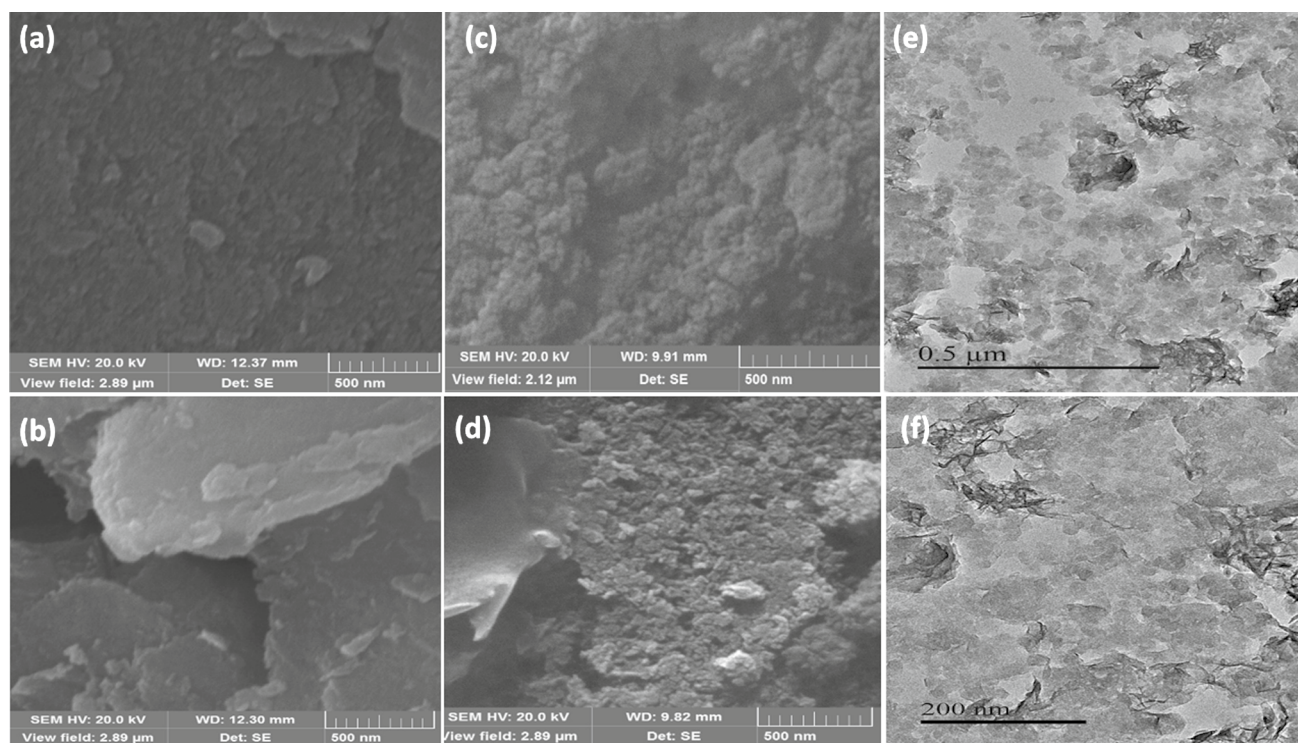


Fig. 2 SEM of NMA (a), G/NMA (b), NMA-C, (c) G/NMA-C (d); TEM images of G/MCA at low magnification (e), high magnification (f)

pH which has a significant effect on the adsorption performance [25, 33]. The influence of pH (range of 2 to 9) on the percent removal of EBT was carried using 0.01 g of adsorbates in 30 mL of 40 mg/L dye solution operated at 180 rpm and 25 °C for 480 min, and results are displayed in Fig. 3a. As depicted, the percent removal of EBT increases as pH increases from 2 to 4. Further increase in pH showed a decrease in EBT removal efficiency except for G/NMA-C which maintains a relatively constant percentage removal at higher pH values. This can be a significant advantage in the practical use of the calcined graphene-LDH composite in dyes removal due to its pH independence when compared to other adsorbents in which performances significantly depend on pH adjustment. The maximum percentage removals recorded for NMA, G/NMA, NMA-C, and G/NMA-C were 88.8, 92.3, 96.5, and 99.3%, respectively. The higher dye removal experienced by calcined graphene-LDH composite was due to the following reasons (1) increased in surface area, (2) formation of mixed metal oxides, providing higher binding sites on the surface of the composite. It is expected that at low pH, protonation of the oxygen functionalities of LDH results in positive surfaces which enhances their interaction with negatively charged anionic

dyes [31]. Further lowering the pH ($\text{pH} < 4$) may expectedly lead to the acid dissolution of adsorbents attributed to the release mechanism of metal ions from LDH structure [16, 34]. The highly polarized surface with weak M–O bonds leads to an increase in dissolution rate of the hydroxide, thus reducing the adsorption performance of the adsorbents. A similar result was demonstrated by Bakr et al. [35] using Co/Mo LDH for Mn removal. At higher pH ($\text{pH} > 6$) values, increasing competition between OH^- and the anionic EBT molecules for the adsorption sites lowers the removal efficiency of the anionic dye [16]. The optimum pH for the adsorption study was 4, and this was used for the rest of the experiment.

3.2.2 Effect of Contact Time

Figure 3b shows the influence of contact time on percentage removal of EBT for a time range of 0 to 480 min. The percentage removal rises with an increase in the contact time with rapid sorption in the first 15 min. This involves physisorption behavior associated with the strong polarity (electrostatic attraction) of the LDH surface leading to rapid attraction of a high number of dye molecules [36, 37]. This

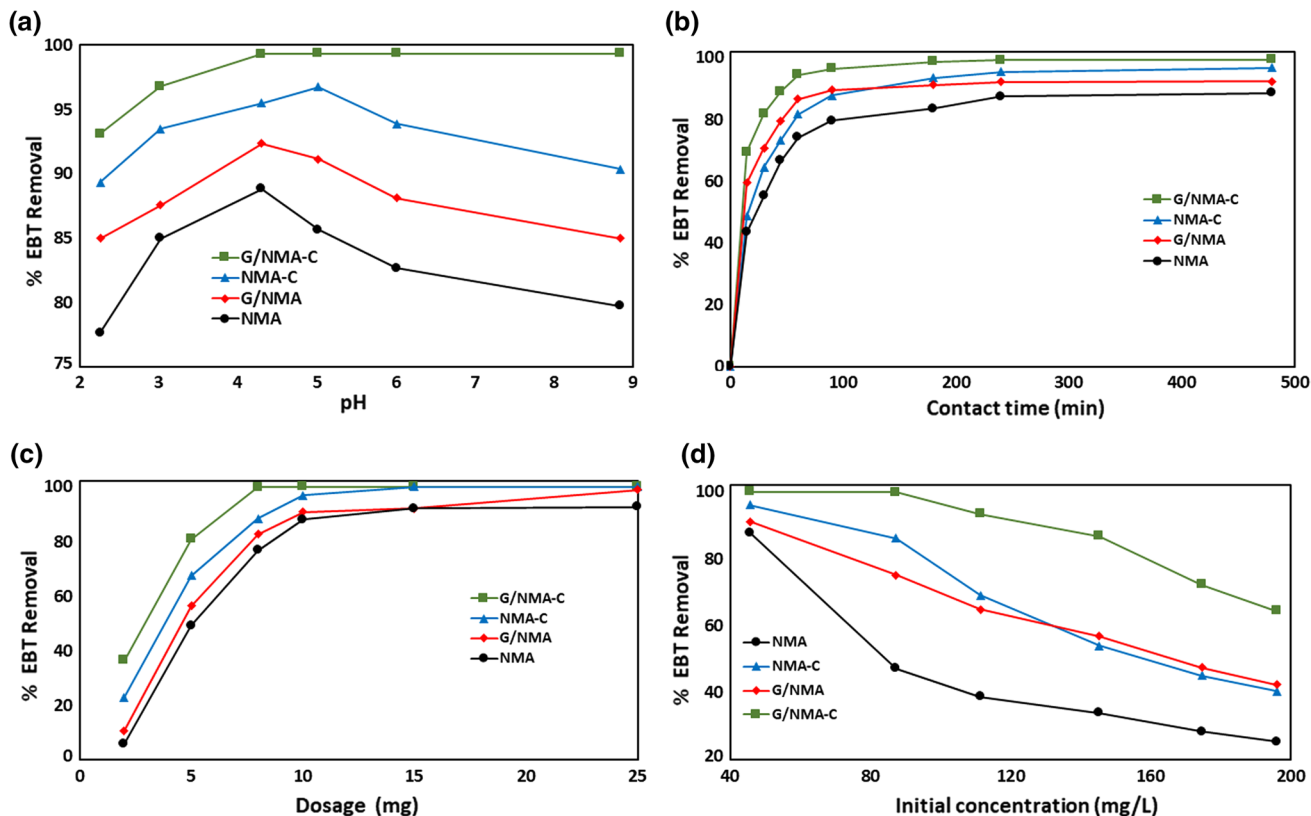


Fig. 3 Effect of pH on percentage removal of EBT (a); effect of contact time on percentage removal of EBT. [Adsorbent dosage 10 mg; $C_0 = 40 \text{ mgL}^{-1}$] (b); effect of dosage on percentage removal of EBT.

[Contact time = 180 min; $C_0 = 40 \text{ mgL}^{-1}$] (c); effect of concentration on percentage removal of EBT. [Contact time = 180 min; adsorbent dosage = 10 mg] (d)

is an indication of the strong polarity of the LDH surface to rapidly attract a high number of dye molecules enhanced by large surface area [36]. Thereafter, the rate gradually reduced until equilibrium was established at 240, 180, 90, and 60 min for NMA, NMA-C, G/NMA, and G/NMA-C, respectively. The faster absorption rate of the graphene-ternary LDH composite compared to the pristine ternary LDH may be due to the higher surface area and functional groups, due to graphene presence, facilitating quick uptake of dyes molecules. In addition, the fast adsorption rate of the calcined composites, compared to the uncalcined composites, can be attributed to memory effect [7, 19].

3.2.3 Effect of Dosage

Figure 3c displays the effect of adsorbents dosages on adsorption of EBT. As shown in Fig. 3c, two stages of adsorption are established. The first stage shows an increase in EBT removal with a rise in adsorbent dosage. This is related to an increase in active adsorption sites with an increased supply of adsorbent. The second stage involves the occurrence of a plateau signifying no further increase in adsorption with increased dosage. This indicated that the number of available adsorption sites exceeds the number of available dye molecules, and thus, there will be excess unadsorbed sites. As shown, the calcined samples recorded higher adsorption performance with increased dosage when compared to its uncalcined counterpart. Likewise, the graphene-ternary composite shows better sorption performance than the pristine ternary LDH which may be associated with the existence of abundant oxygen functionalities and specific surface area resulting in increased active binding sites for dyes adsorption. In detail, an increase in adsorbent dosage from 2 to 10 mg resulted in percentage increase of EBT adsorption from 6, 23, 11, and 36 to 87, 91, 96, and 99% for NMA, G/NMA, NMA-C, and G/NMA-C, respectively.

For calcined G-LDH, percentage removal plateaus at 10 mg, whereas G/NMA showed increased adsorption with adsorbent dosage. On the other hand, both NMA and NMA-C establish a plateau at 15 mg for removal of 92% and 99% EBT, respectively. This shows the superior advantage of calcined graphene-LDH which possesses synergistic properties of hybridization and calcination.

3.2.4 Effect of EBT Concentration

Figure 3(d) shows the effect of initial EBT concentration on the percentage removal of dye. As the initial concentration of dye increases, the percentage removal reduces. Since the adsorbent dosage is fixed, the number of adsorption sites is fully saturated with dyes molecules rendering more dye molecules unadsorbed as the initial dye concentration is increased. This thus causes a reduction of percentage removal with an increase in initial dye concentration [16]. The percentage removal of EBT decreased from 87.8, 91.1, 96.1, and 99.9 to 34.0, 64.9, 69.0, and 93.3% for NMA, G/NMA, NMA-C, and calcined G/NMA-C, respectively, when initial dye concentration increased from 45 to 110 mg/L. The results further confirm that the graphene with ternary LDH showed higher performance in adsorbing EBT.

3.3 Isotherm Studies

The three isotherms are fitted to the experimental data, and the parameters obtained are listed in Table 2. Figure 4a–c displays the linear plots of all the three considered models. As shown in Table 2, Langmuir isotherm model showed highest correlation coefficient ($R^2 > 0.99$) in comparison with Freundlich ($R^2 > 0.94$) and Temkin isotherm ($R^2 > 0.89$) for all adsorbents (NMA, G/NMA, NMA-C, and G/NMA-C) and temperatures (25–45) °C. This demonstrated that the distribution of EBT molecules on the surface of sorbents

Table 2 Parameters of isotherm models for adsorption of EBT

Sample	T (K)	Langmuir			Freundlich			Temkin		
		q_m (mg/g)	R_L	R^2	K_F	$1/n$	R^2	$A \times 10^{-3}$	B	R^2
NMA	298	156.25	0.035	0.992	104.18	0.06	0.699	9.282	8.84	0.681
	308	136.97	0.026	0.997	98.31	0.05	0.967	9.636	96.00	0.956
	323	126.97	0.030	0.999	84.15	0.07	0.994	3.947	7.69	0.995
G/NMA	298	263.16	0.031	0.998	95.89	0.21	0.964	6.231	39.54	0.977
	308	256.41	0.067	0.979	94.01	0.17	0.953	10.93	30.83	0.944
	323	217.39	0.067	0.992	90.30	0.15	0.970	23.34	24.28	0.977
NMA-C	298	238.14	0.022	0.997	146.79	0.11	0.866	1.312	20.81	0.882
	308	204.23	0.019	0.984	122.51	0.09	0.991	1.276	16.33	0.993
	323	188.68	0.017	0.988	107.10	0.11	0.968	4.498	16.69	0.985
G/NMA-C	298	384.62	0.002	0.999	283.79	0.07	0.983	1.381	18.35	0.972
	308	370.37	0.018	0.997	248.42	0.08	0.974	1.661	18.41	0.988
	323	322.58	0.024	0.997	227.24	0.06	0.973	1.109	14.69	0.993

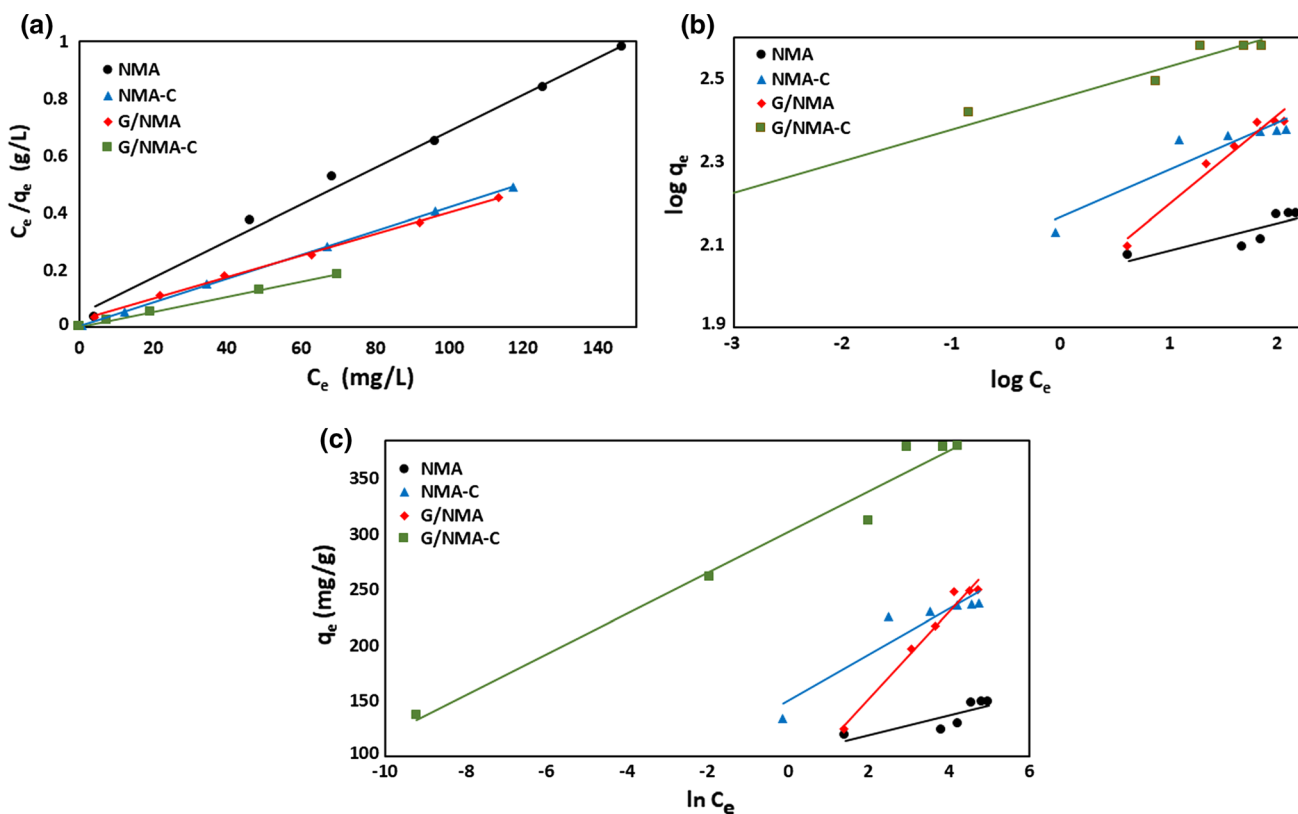


Fig. 4 a Langmuir, b Freundlich, and c Temkin isotherm models for NMA, NMA-C, G/NMA, and G/NMA-C at 298 K

involves monolayer adsorption phenomena as assumed by Langmuir model [24]. The maximum adsorption capacities, computed at 25 °C, are 156.25 mg/g, 263.16 mg/g, 238.14 mg/g, and 384.62 mg/g for NMA, G/NMA, NMA-C, and G/NMA-C, respectively. The highest adsorption performance of G/MCA-C is attributed to substantial improvement in surface and structure characteristics of ternary LDH after incorporation of graphene and calcination which facilitated the removal of EBT dye molecules from the water phase. The values of R_L estimated using Eq. 5 vary with temperature and ranged from 0.0350 to 0.0020 at 25 °C, 0.0265 to 0.0180 at 35 °C, and 0.0307 to 0.0241 at 45 °C for NMA, G/NMA, NMA-C, and G/NMA-C composites, respectively. These results concluded that, at all temperatures, the sorption of EBT is favorable.

3.4 Kinetic Studies

The kinetic parameters calculated from the linear regression using the above equations and the correlation coefficients are summarized in Table 3. Figure 5a–d shows the linear plots of the PFO, PSO, IPD, and Elovich models. Table 3 shows that the correlation coefficient (R^2) for all adsorbents is found in order PSO > IDP > Elovich > PFO. This demonstrated that the rate of adsorption of EBT molecules onto ternary LDH

and graphene-ternary LDH composite is well described by the PSO model with the highest correlation coefficient ($R^2 > 0.99$). In addition, the $q_{e,cal}$ obtained from the PSO model was close to the experimental value, $q_{e,exp}$. Therefore, it can be stated that the dominating rate-controlling mechanism is predominated by chemisorption [38]. Similar results have been reported concluding chemisorption as the main controlling step in the removal of anionic dyes by various LDHs [3, 31, 32, 39, 40].

3.5 Effect of Temperature and Thermodynamic Studies

The thermodynamic study was undertaken to know the effects of temperature on the adsorption process via changes in enthalpy (ΔH), Gibb’s free energy (ΔG), and entropy (ΔS) according to the following relations

$$\Delta G = -RT \ln K_D \tag{16}$$

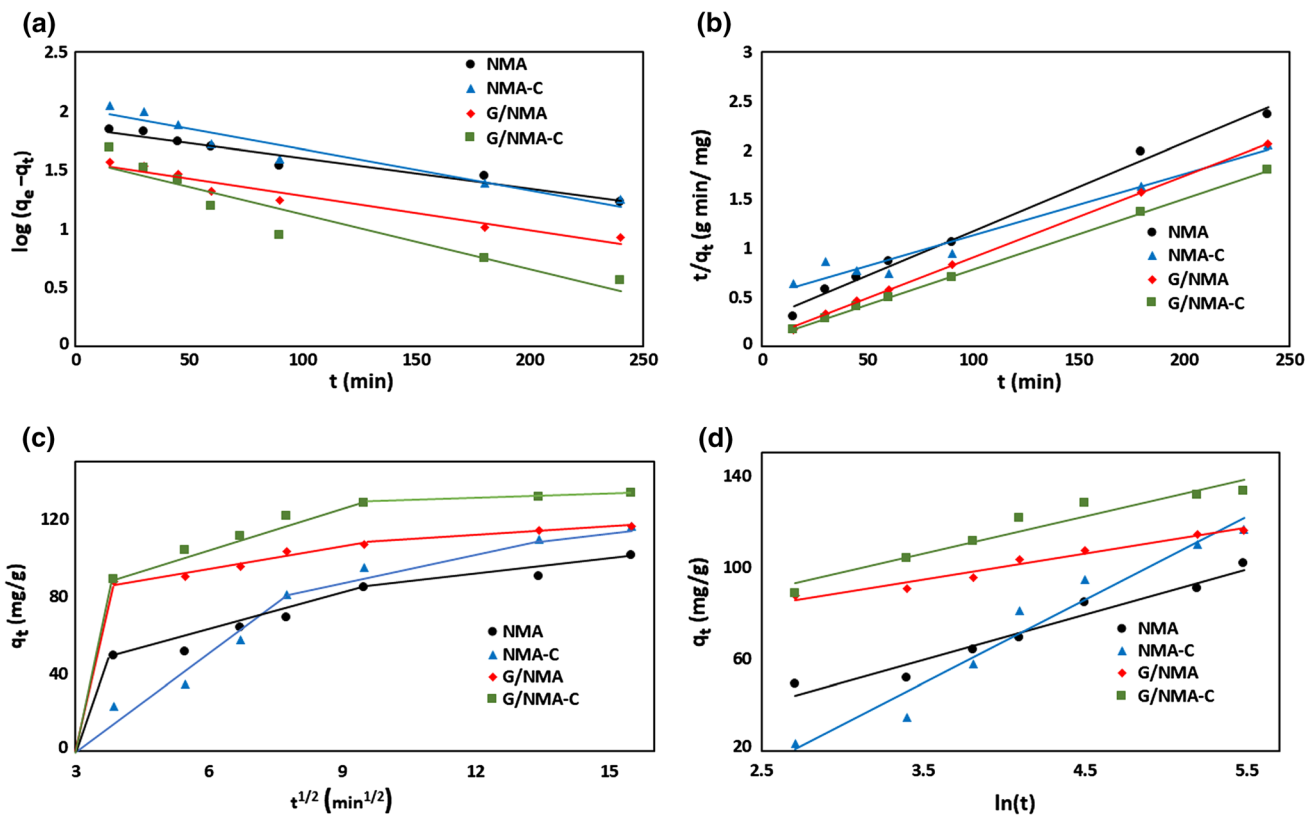
$$\ln K_D = \frac{\Delta S}{R} - \frac{\Delta H}{RT} \tag{17}$$

where T (K) is absolute temperature and R (8.314 J/mol/K) is molar gas constant. K_D (L/g) is a thermodynamic equilibrium

Table 3 Parameters of kinetic models for adsorption of EBT onto NMA and G/NMA composites

Adsorbent	q_e (exp)	Pseudo-first order			Pseudo-second order		
		q_e (cal)	k_1	R^2	q_e (cal)	$k_2 * 10^{-2}$	R^2
NMA	118.50	72.23	0.006	0.951	111.11	2.95	0.991
G/NMA	124.76	37.16	0.006	0.949	120.48	8.87	0.999
NMA-C	134.34	106.29	0.008	0.933	161.29	0.76	0.960
G/NMA-C	137.02	39.26	0.010	0.899	138.88	7.86	0.999

	IPD			Elovich		
	K_d	C	R^2	α	β	R^2
NMA	4.58	32.20	0.945	12.03	0.05	0.952
G/NMA	2.57	79.31	0.931	1428.19	0.08	0.965
NMA-C	8.12	1.87	0.888	4.30	0.02	0.956
G/NMA-C	3.48	85.93	0.802	339.40	0.06	0.928

**Fig. 5** a Pseudo-first-order, b pseudo-second-order, c intraparticle diffusion, d Elovich models for NMA, G/NMA, NMA-C, and G/NMA-C at 298 K

constant defined as distribution coefficient which is obtained by plotting $\ln(q_e/C_e)$ versus q_e and extrapolating q_e to zero [32]. ΔG is estimated from Eq. (16), while ΔH and ΔS are computed from the slope and intercept of the linear plot of $\ln K_D$ versus $1/T$ in Eq. 17. The thermodynamic variables are documented in Table 4 based on the three temperatures used (298, 308, and 318 K).

The adsorption of EBT on all the as-synthesized adsorbents is thermodynamically feasible and spontaneous with a strong affinity between the EBT molecules and all adsorbents as indicated by a negative value of ΔG [41]. The value of ΔG increased from -6.60 to -6.23 (NMA), -5.96 to -4.82 (NMA-C), -4.39 to -4.03 (G/NMA), and -7.47 to -5.36 (G/NMA-C) when the temperature

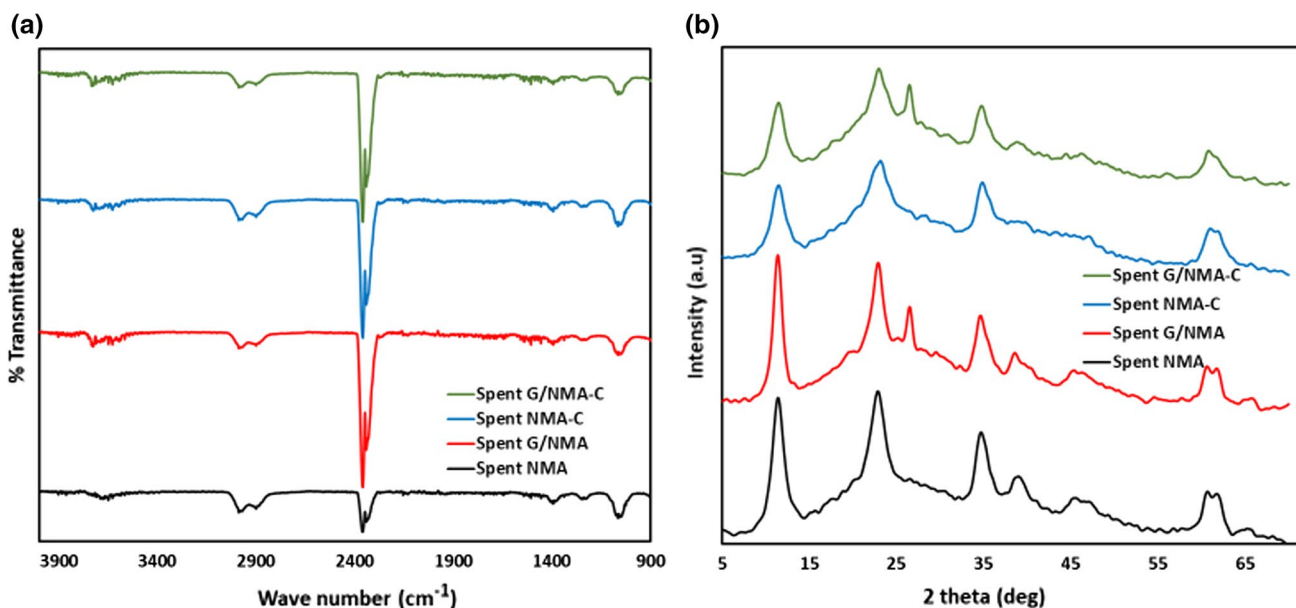
Table 4 Thermodynamics parameters for adsorption of EBT onto NMA and G/NMA composites

Sample	T (K)	K_D	ΔG (kJ/mol)	ΔH (kJ/mol)	ΔS (J/mol K)
NMA	298	14.38	-6.60	-10.63	-14.08
	308	10.42	-6.00		
	323	10.13	-6.23		
NMA-C	298	11.07	-5.96	-20.01	-46.62
	308	10.11	-5.92		
	323	6.03	-4.82		
G/NMA	298	5.87	-4.39	-6.58	-7.70
	308	4.83	-4.03		
	323	4.73	-4.17		
G/NMA-C	298	20.40	-7.47	-30.96	-80.58
	308	8.25	-5.40		
	323	7.35	-5.36		

was increased from 298 to 318 K, showing an exothermic process. This was further confirmed by the decline in adsorption capacity with an increase in temperature (Table 2) and negative values of ΔH for all adsorbents. In addition, the negative values of ΔS for NMA (-14.08), NMA-C (-46.62), G/NMA (-7.70), and G/NMA-C (80.58), describe a greater order of reaction during the EBT adsorption. Similar conclusions have been reported in previous relevant studies.

3.6 Adsorption Mechanism

From FTIR spectra of Fig. 6a, the reduction and shift of the peak from 3440 cm^{-1} to about 3690 cm^{-1} assigned to the stretching vibration of interlayer water and the disappearance of the peak at 1640 cm^{-1} assigned to the bending mode of interlayer water molecules suggest a contribution of hydrogen bonding in the adsorption process [42]. In addition, the weakening of the strong band at 1350 cm^{-1} associated with nitrate ion as well as the emergence of new peaks between 2400 and 2900 cm^{-1} suggests the interplay of chemical and electrostatic interaction between the adsorbents surfaces and the EBT dye molecules. Figure 6b shows the XRD of the spent adsorbents which shows no significant shift in the positions of diffraction peaks when compared to fresh samples (Fig. 1a), implying no intercalation of anionic EBT molecules into the LDH, but rather surface adsorption of the dye molecules onto the LDH indicates more random crystal deformation [43, 44]. The XRD patterns of used calcined samples display peaks assigned to d_{003} and d_{006} similar to their original LDHs which form through rehydration and surface reconstruction upon contact with an aqueous solution. The peaks were broad with decreased intensity implying reduced crystallinity. The calcined samples regained their original LDH structure through memory effect upon rehydration. Structural reconstruction via ‘memory effect’ along with surface adsorption forms the basis of dye removal by NMA-C and G/MCA-C. Figure 7 shows the microstructure of adsorbents after EBT adsorption. It was observed that the surface of all the adsorbents transformed into very smooth and flat surface morphology after EBT adsorption.

**Fig. 6** FTIR of spent NMA, G/NMA, NMA-C, and G/NMA-C (a); XRD of spent NMA, G/NMA, NMA-C, and G/NMA-C (b)

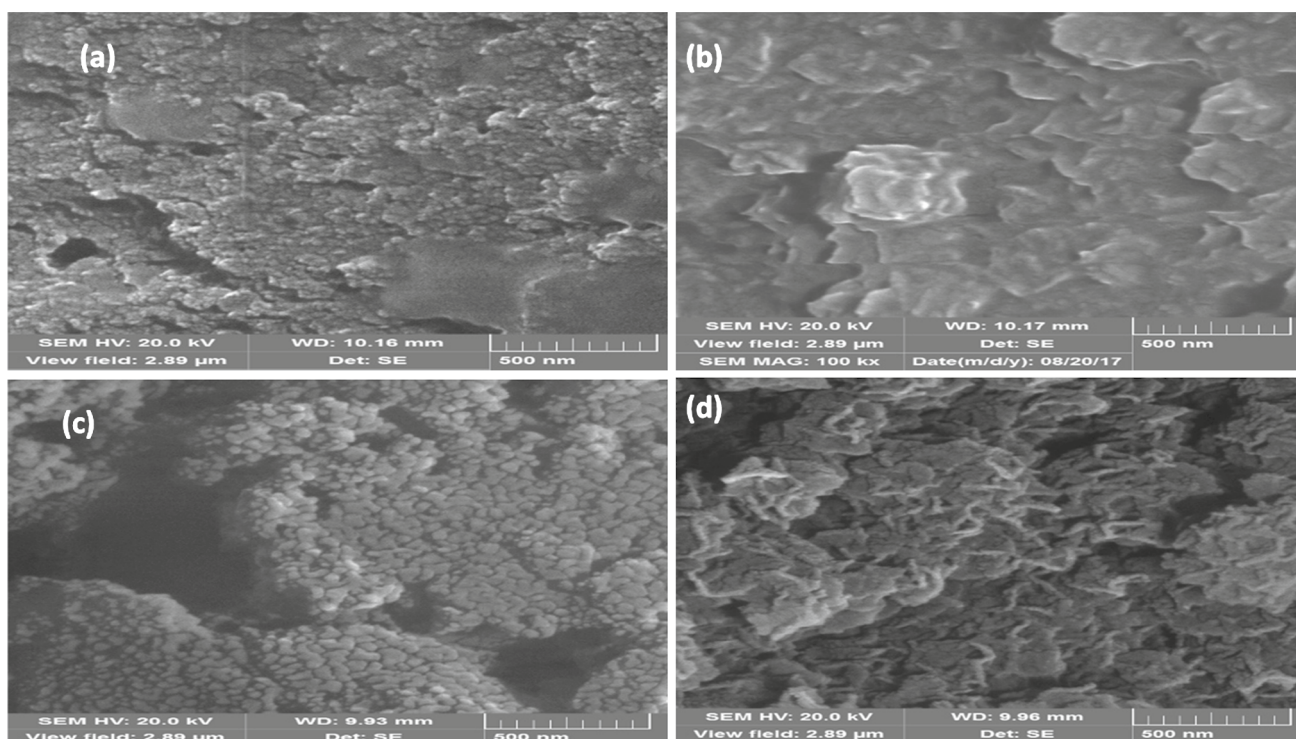


Fig. 7 SEM of spent **a** NMA, **b** G/NMA, **c** NMA-C, and **d** G/NMA-C

This indicated that the EBT molecules were homogeneously distributed on the surface of the adsorbent, resulting in entire coverage of binding sites on the surface of the adsorbent. Therefore, based on the results, the mechanism of adsorption of EBT molecules onto uncalcined composites involves surface adsorption, strong electrostatic interaction, and chemical bonding between EBT anions and adsorbent oxygen functionalities, whereas along with these, structural reconstruction (memory effect) was also dominant for the calcined composites.

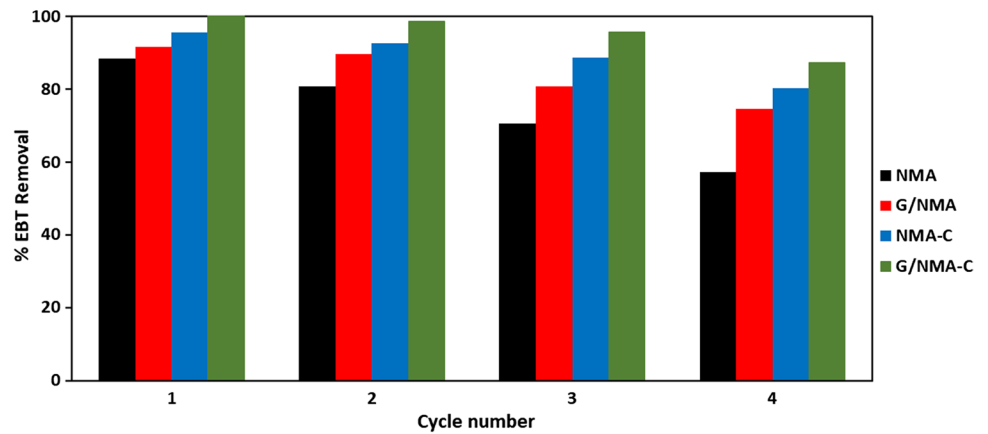
3.7 Regeneration and Reuse of Adsorbents

Regeneration and reuse account for a substantial part (> 70%) of operating and maintenance cost [45]. Hence, great consideration is given toward choosing materials for the economic feasibility of any process. Due to anionic nature of the dye, an alkaline solution can desorb the dyes molecules by weakening the electrostatic attraction between the surfaces of adsorbents and the dye [46]. 0.1 M NaOH solution was employed to regenerate the adsorbent. In addition to the basic treatment, calcination at 500 °C for 4 h under nitrogen environment was used to regenerate the spent calcined NiMgAl and its graphene hybrid. For subsequent regeneration, the same desorption and calcination treatments were employed. After each regeneration

procedure, the adsorbents were directly applied to the EBT dye solution adjusted to pH 4 (pH used throughout the study). Figure 8 shows EBT dye removal after each cycle reuse and regeneration. On NMA, the percentage of EBT removed decreased from 88 to 81% in the first 2 cycles and reached 57% at the end of the fourth cycle. G/NMA reached 74% removal efficiency at the end of the fourth cycle. This lesser reduction may be due to the influence of graphene in the LDH structure. After each regeneration cycle, there is continual loss of surface area on the regenerated adsorbents when compared to fresh adsorbents due to irreversible and permanent adsorption of some of the dye molecules onto the surface of the adsorbent which will inherently result in reduction adsorption inefficiency. Comparing the FTIR plots (Fig. S3) between the fresh and used adsorbents, there is a significant reduction in the peaks on the oxygen-carrying functional groups on the spent adsorbents. This occurrence denotes the continuous loss of adsorption performance on the materials with each regeneration cycle as observed in Fig. 8. Calcination helped improved the recovery of the adsorbent as NMA-C and G/NMA-C had percentage removal of 80% and 87% at the end of the fourth cycle. This implies the regeneration of the adsorbents was efficient, and they could be deployed as affordable reusable adsorbents.



Fig. 8 Percentage removal of EBT dye adsorbents after four regeneration cycles



3.8 Comparison with the Literature

Table 5 compares the maximum adsorption capacity of the adsorbents synthesized in this work with other conventional adsorbents previously reported in the literature. It clearly shows that those from this work exhibits superior performances than others, implying it could be deployed for the remediation of anionic dye-contaminated water. The higher performances may be attributed to the synthesis techniques which facilitated the formation of abundant function groups of oxygen, and higher surface area resulting from calcination [47, 48] was further improved by hybridizing the LDH with graphene.

4 Conclusion

We have established in this study the potentiality of use ternary LDH (NMA) and graphene-ternary LDH (G/NMA) along with their calcined products, NMA-C, and G/NMA-C, in the removal of an azo dye, EBT, from an aqueous solution. Structural characterizations of the adsorbents by FTIR and XRD show the presence of abundant oxygen

functionalities and excellent integration of graphene and LDH. The characterization techniques also showed the formation of layered double oxide (LDO) after calcination. Addition of graphene significantly improves the surface functionalities and surface area of NMA which facilitates the dye uptake performance. The parametric studies reveal that the optimum pH is 4, the optimum dosage is 10 mg, and equilibrium was established from 60 min for G/NMA-C and 180 min for NMA. It was further revealed that the adsorption on calcined graphene-ternary LDH composite (G/NMA-C) was highly pH-independent which makes it more promising for industrial application. Isotherm study also revealed that Langmuir isotherm better qualifies the adsorption process with a maximum adsorption capacity of 156.25, 263.16, 238.14, and 384.62 mg/g for NMA, G/NMA, NMA-C, and G/NMA-C, respectively. The kinetic study indicated the suitability of the pseudo-second-order model. The thermodynamic evaluation showed the exothermic nature of the adsorption with lower adsorption at a higher temperature. The adsorption mechanism of EBT-graphene-ternary LDH composite follows surface adsorption, hydrogen bonding, and chemical interactions between dyes molecules and surface functional groups. The adsorbents are easily recovered

Table 5 Comparison of capacity and parameters of various adsorbents for EBT adsorption

Adsorbent	pH	Time (min)/temp (°C)	Models	q_m (mg/g)	References
Bottom ash	3.5	270/40	Langmuir/2nd	94.122	[49]
Activated carbon	2		Freundlich/2nd	160	[50]
Almond shell MW irradiated	4	180/30	Langmuir/2nd	29.41	[51]
Acid-modified graphene	2–4		Langmuir/2nd	128	[52]
Eucalyptus bark	2	–/30		52.36	[53]
Date palm ash/MgAl	2	180/25	Langmuir/2nd	167.84	[40]
NMA	4	180/25	Langmuir/2nd	156.25	This work
G/NMA	4	180/25	Langmuir/2nd	263.16	This work
NMA-C	4	180/25	Langmuir/2nd	238.14	This work
G/NMA-C	4	180/25	Langmuir/2nd	384.62	This work

with high reusability up to the 4th cycle, indicating their potential for industrial applications. Calcined graphene-ternary LDH composite showed superb removal performance of EBT dye and is attributed to the synergistic effect of hybridization and calcination.

Acknowledgements The authors acknowledge the Centre for Nanotechnology (CENT) and the Department of Chemical Engineering, KFUPM, for their support toward the completion of this work.

References

- Jain, S.N.; Gogate, P.R.: Acid Blue 113 removal from aqueous solution using novel biosorbent based on NaOH treated and surfactant modified fallen leaves of *Prunus Dulcis*. *J. Environ. Chem. Eng.* **5**(4), 3384–3394 (2017). <https://doi.org/10.1016/j.jece.2017.06.047>
- Hasmath Farzana, M.; Meenakshi, S.: Decolorization and detoxification of Acid blue 158 dye using cuttlefish bone powder as co-adsorbent via photocatalytic method. *J. Water Process Eng.* **2**(Supplement C), 22–30 (2014). <https://doi.org/10.1016/j.jwpe.2014.03.010>
- Zubair, M.; Jarrah, N.; Ihsanullah, K.A.; Manzar, M.S.; Kazeem, T.S.; Al-Harathi, M.A.: Starch-NiFe-layered double hydroxide composites: efficient removal of methyl orange from aqueous phase. *J. Mol. Liq.* **249**, 254–264 (2018). <https://doi.org/10.1016/j.molliq.2017.11.022>
- Rao, R.A.K.; Kashifuddin, M.: Kinetics and isotherm studies of Cd (II) adsorption from aqueous solution utilizing seeds of bottlebrush plant (*Callistemon chisholmii*). *Appl. Water Sci.* **4**(4), 371–383 (2014)
- Khan, M.A.; Uddin, M.K.; Bushra, R.; Ahmad, A.; Nabi, S.A.: Synthesis and characterization of polyaniline Zr(IV) molybdophosphate for the adsorption of phenol from aqueous solution. *React. Kinet. Mech. Catal.* **113**(2), 499–517 (2014)
- Zubair, M.; Daud, M.; McKay, G.; Shehzad, F.; Al-Harathi, M.A.: Recent progress in layered double hydroxides (LDH)-containing hybrids as adsorbents for water remediation. *Appl. Clay Sci.* **143**, 279–292 (2017). <https://doi.org/10.1016/j.clay.2017.04.002>
- Goh, K.-H.; Lim, T.-T.; Dong, Z.: Application of layered double hydroxides for removal of oxyanions: a review. *Water Res.* **42**(6–7), 1343–1368 (2008)
- Daud, M.; Kamal, M.S.; Shehzad, F.; Al-Harathi, M.A.: Graphene/layered double hydroxides nanocomposites: a review of recent progress in synthesis and applications. *Carbon* **104**, 241–252 (2016)
- Li, J.; Zhang, N.; Ng, D.H.: Synthesis of a 3D hierarchical structure of γ -AlO(OH)/Mg–Al-LDH/C and its performance in organic dyes and antibiotics adsorption. *J. Mater. Chem. A* **3**(42), 21106–21115 (2015)
- Khodam, F.; Rezvani, Z.; Amani-Ghadim, A.R.: Enhanced adsorption of acid red 14 by co-assembled LDH/MWCNTs nanohybrid: optimization, kinetic and isotherm. *J. Ind. Eng. Chem.* **21**, 1286–1294 (2015)
- Garcia-Gallastegui, A.; Iruretagoyena, D.; Mokhtar, M.; Asiri, A.M.; Basahel, S.N.; Al-Thabaiti, S.A.; Alyoubi, A.O.; Chadwick, D.; Shaffer, M.S.: Layered double hydroxides supported on multi-walled carbon nanotubes: preparation and CO₂ adsorption characteristics. *J. Mater. Chem.* **22**(28), 13932–13940 (2012)
- Zhang, M.; Yao, Q.; Lu, C.; Li, Z.; Wang, W.: Layered double hydroxide–carbon dot composite: high-performance adsorbent for removal of anionic organic dye. *ACS Appl. Mater. Interfaces* **6**(22), 20225–20233 (2014)
- Wang, J.; Mei, X.; Huang, L.; Zheng, Q.; Qiao, Y.; Zang, K.; Mao, S.; Yang, R.; Zhang, Z.; Gao, Y.: Synthesis of layered double hydroxides/graphene oxide nanocomposite as a novel high-temperature CO₂ adsorbent. *J. Energy Chem.* **24**(2), 127–137 (2015)
- Cao, Y.; Li, G.; Li, X.: Graphene/layered double hydroxide nanocomposite: properties, synthesis, and applications. *Chem. Eng. J.* **292**, 207–223 (2016)
- Bharali, D.; Deka, R.C.: Preferential adsorption of various anionic and cationic dyes from aqueous solution over ternary CuMgAl layered double hydroxide. *Colloids Surf. A* **525**(Supplement C), 64–76 (2017). <https://doi.org/10.1016/j.colsurfa.2017.04.060>
- Zaghouane-Boudiaf, H.; Boutahala, M.; Arab, L.: Removal of methyl orange from aqueous solution by uncalcined and calcined MgNiAl layered double hydroxides (LDHs). *Chem. Eng. J.* **187**, 142–149 (2012). <https://doi.org/10.1016/j.cej.2012.01.112>
- Chowdhury, P.R.; Bhattacharyya, K.G.: Ni/Co/Ti layered double hydroxide for highly efficient photocatalytic degradation of Rhodamine B and Acid Red G: a comparative study. *Photochem. Photobiol. Sci.* **16**(6), 835–839 (2017)
- Pan, D.; Ge, S.; Zhao, J.; Shao, Q.; Guo, L.; Zhang, X.; Lin, J.; Xu, G.; Guo, Z.: Synthesis, characterization and photocatalytic activity of mixed-metal oxides derived from NiCoFe ternary layered double hydroxides. *Dalton Trans.* **47**(29), 9765–9778 (2018)
- Yuan, X.; Wang, Y.; Wang, J.; Zhou, C.; Tang, Q.; Rao, X.: Calcined graphene/MgAl-layered double hydroxides for enhanced Cr(VI) removal. *Chem. Eng. J.* **221**, 204–213 (2013)
- Ruan, X.; Chen, Y.; Chen, H.; Qian, G.; Frost, R.L.: Sorption behavior of methyl orange from aqueous solution on organic matter and reduced graphene oxides modified Ni–Cr layered double hydroxides. *Chem. Eng. J.* **297**(Supplement C), 295–303 (2016). <https://doi.org/10.1016/j.cej.2016.01.041>
- Newman, S.P.; Jones, W.: Synthesis, characterization and applications of layered double hydroxides containing organic guests. *New J. Chem.* **22**(2), 105–115 (1998)
- Kazeem, T.S.; Lateef, S.A.; Ganiyu, S.A.; Qamaruddin, M.; Tanimu, A.; Sulaiman, K.O.; Jillani, S.M.S.; Alhooshani, K.: Aluminium-modified activated carbon as efficient adsorbent for cleaning of cationic dye in wastewater. *J. Clean. Prod.* **205**, 303–312 (2018)
- Monash, P.; Pugazhenthii, G.: Utilization of calcined Ni–Al layered double hydroxide (LDH) as an Adsorbent for removal of methyl orange dye from aqueous solution. *Environ. Progress Sustain. Energy* **33**(1), 154–159 (2014)
- Vimonses, V.; Lei, S.; Jin, B.; Chow, C.W.; Saint, C.: Kinetic study and equilibrium isotherm analysis of Congo Red adsorption by clay materials. *Chem. Eng. J.* **148**(2), 354–364 (2009)
- Lafi, R.; Charradi, K.; Djebbi, M.A.; Amara, A.B.H.; Hafiane, A.: Adsorption study of Congo red dye from aqueous solution to Mg–Al-layered double hydroxide. *Adv. Powder Technol.* **27**(1), 232–237 (2016)
- Ahmed, I.; Gasser, M.: Adsorption study of anionic reactive dye from aqueous solution to Mg–Fe–CO₃ layered double hydroxide (LDH). *Appl. Surf. Sci.* **259**, 650–656 (2012)
- Zandipak, R.; Sobhanardakani, S.: Synthesis of NiFe₂O₄ nanoparticles for removal of anionic dyes from aqueous solution. *Desalin. Water Treat.* **57**(24), 11348–11360 (2016)
- Iruretagoyena, D.; Shaffer, M.S.P.; Chadwick, D.: Layered double oxides supported on graphene oxide for CO₂ adsorption: effect of support and residual sodium. *Ind. Eng. Chem. Res.* **54**, 6781–6792 (2015)
- Zhang, Z.-Q.; Liao, M.-C.; Zeng, H.-Y.; Xu, S.; Liu, X.-J.; Du, J.-Z.; Zhu, P.-H.; Huang, Q.-J.: Temperature effect on chromium(VI) removal by Mg/Al mixed metal oxides as adsorbents. *Appl. Clay Sci.* **102**, 246–253 (2014). <https://doi.org/10.1016/j.clay.2014.10.005>

30. Sumari, S.M.; Hamzah, Z.; Kantasamy, N.: Adsorption of anionic dyes from aqueous solutions by calcined and uncalcined Mg/Al layered double hydroxide. *Malays. J. Anal. Sci.* **20**(4), 777–792 (2016)
31. Zubair, M.; Jarrah, N.; Manzar, M.S.; Al-Harhi, M.; Daud, M.; Mu'azu, N.D.; Haladu, S.A.: Adsorption of eriochrome black T from aqueous phase on MgAl-, CoAl- and NiFe- calcined layered double hydroxides: kinetic, equilibrium and thermodynamic studies. *J. Mol. Liq.* **230**, 344–352 (2017). <https://doi.org/10.1016/j.molliq.2017.01.031>
32. Kazeem, T.S.; Zubair, M.; Daud, M.; Mu'azu, N.D.; Al-Harhi, M.A.: Graphene/ternary layered double hydroxide composites: efficient removal of anionic dye from aqueous phase. *Korean J. Chem. Eng.* **36**(7), 1057–1068 (2019)
33. Liu, J.; Li, X.; Luo, J.; Duan, C.; Hu, H.; Qian, G.: Enhanced decolourisation of methylene blue by LDH-bacteria aggregates with bioregeneration. *Chem. Eng. J.* **242**, 187–194 (2014)
34. Deng, L.; Shi, Z.; Peng, X.; Zhou, S.: Magnetic calcinated cobalt ferrite/magnesium aluminum hydrotalcite composite for enhanced adsorption of methyl orange. *J. Alloys Compd.* **688**, 101–112 (2016)
35. Bakr, A.; Mostafa, M.; Sultan, E.: Mn(II) removal from aqueous solutions by Co/Mo layered double hydroxide: kinetics and thermodynamics. *Egypt. J. Petrol.* **25**(2), 171–181 (2016)
36. Ahmed, M.; Mohamed, A.: An efficient adsorption of indigo carmine dye from aqueous solution on mesoporous Mg/Fe layered double hydroxide nanoparticles prepared by controlled sol-gel route. *Chemosphere* **174**, 280–288 (2017)
37. Flores, L.H.C.; Debut, A.; Stael, C.: Synthesis of multicomponent nanoparticles for immobilization of heavy metals in aqueous phase. *NanoWorld J.* **1**, 105–111 (2015)
38. Ho, Y.S.; McKay, G.: Pseudo-second order model for sorption processes. *Process. Biochem.* **34**(5), 451–465 (1999). [https://doi.org/10.1016/S0032-9592\(98\)00112-5](https://doi.org/10.1016/S0032-9592(98)00112-5)
39. Mu'azu, N.D.; Jarrah, N.; Kazeem, T.S.; Zubair, M.; Al-Harhi, M.: Bentonite-layered double hydroxide composite for enhanced aqueous adsorption of eriochrome black T. *Appl. Clay Sci.* **161**, 23–34 (2018). <https://doi.org/10.1016/j.clay.2018.04.009>
40. Blaisi, N.I.; Zubair, M.; Ihsanullah, Ali, S.; Kazeem, T.S.; Manzar, M.S.; Al-Kutti, W.; Al Harhi, M.A.: Date palm ash-MgAl-layered double hydroxide composite: sustainable adsorbent for effective removal of methyl orange and eriochrome black-T from aqueous phase. *Environ. Sci. Pollut. Res.* **25**(34), 34319–34331 (2018)
41. Extremera, R.; Pavlovic, I.; Pérez, M.; Barriga, C.: Removal of acid orange 10 by calcined Mg/Al layered double hydroxides from water and recovery of the adsorbed dye. *Chem. Eng. J.* **213**, 392–400 (2012)
42. Jin, Z.; Wang, X.; Sun, Y.; Ai, Y.; Wang, X.: Adsorption of 4-*n*-nonylphenol and bisphenol-A on magnetic reduced graphene oxides: a combined experimental and theoretical studies. *Environ. Sci. Technol.* **49**(15), 9168–9175 (2015). <https://doi.org/10.1021/acs.est.5b02022>
43. Wang, J.; Kang, D.; Yu, X.; Ge, M.; Chen, Y.: Synthesis and characterization of Mg–Fe–La trimetal composite as an adsorbent for fluoride removal. *Chem. Eng. J.* **264**(Supplement C), 506–513 (2015). <https://doi.org/10.1016/j.cej.2014.11.130>
44. Xiang, W.; Zhang, G.; Zhang, Y.; Tang, D.; Wang, J.: Synthesis and characterization of cotton-like Ca–Al–La composite as an adsorbent for fluoride removal. *Chem. Eng. J.* **250**(Supplement C), 423–430 (2014). <https://doi.org/10.1016/j.cej.2014.03.118>
45. Samuei, S.; Rezvani, Z.; Amani-Ghadim, A.R.: Comparative study of removal of reactive dye by LDHs: the effect of cation variety. *Environ. Progress. Sustain. Energy* **36**(2), 372–381 (2017)
46. Ngwabebhoh, F.A.; Gazi, M.; Oladipo, A.A.: Adsorptive removal of multi-azo dye from aqueous phase using a semi-IPN superabsorbent chitosan-starch hydrogel. *Chem. Eng. Res. Des.* **112**, 274–288 (2016)
47. Teixeira, T.P.F.; Aquino, S.; Pereira, S.; Dias, A.: Use of calcined layered double hydroxides for the removal of color and organic matter from textile effluents: kinetic, equilibrium and recycling studies. *Braz. J. Chem. Eng.* **31**(1), 19–26 (2014)
48. Bharali, D.; Devi, R.; Bharali, P.; Deka, R.C.: Synthesis of high surface area mixed metal oxide from the NiMgAl LDH precursor for nitro-aldol condensation reaction. *New J. Chem.* **39**(1), 172–178 (2015). <https://doi.org/10.1039/C4NJ01332H>
49. Mittal, A.; Gupta, V.K.: Adsorptive removal and recovery of the azo dye eriochrome black T. *Toxicol. Environ. Chem.* **92**(10), 1813–1823 (2010)
50. de Luna, M.D.G.; Flores, E.D.; Genuino, D.A.D.; Futralan, C.M.; Wan, M.-W.: Adsorption of eriochrome black T (EBT) dye using activated carbon prepared from waste rice hulls—optimization, isotherm and kinetic studies. *J. Taiwan Inst. Chem. Eng.* **44**(4), 646–653 (2013)
51. Şahin, Ö.; Saka, C.; Kutluay, S.: Cold plasma and microwave radiation applications on almond shell surface and its effects on the adsorption of eriochrome black T. *J. Ind. Eng. Chem.* **19**(5), 1617–1623 (2013)
52. Khalid, A.; Zubair, M.; Ihsanullah: a comparative study on the adsorption of eriochrome black T dye from aqueous solution on graphene and acid-modified graphene. *Arab. J. Sci. Eng.* **43**(5), 2167–2179 (2018). <https://doi.org/10.1007/s13369-017-2543-x>
53. Khurana, I.; Shaw, A.K.; Khurana, J.M.; Rai, P.K.: Batch and dynamic adsorption of eriochrome black T from water on magnetic graphene oxide: experimental and theoretical studies. *J. Environ. Chem. Eng.* **6**(1), 468–477 (2018)

